Kinetics of a twinning step

Lifeng Liu, Anna Vainchtein and YangYang Wang

Mathematics and Mechanics of Solids published online 24 June 2013
DOI: 10.1177/1081286513490187

Article

MMS

Mathematics and Mechanics of Solids
1–20

DOI: 10.1177/1081286513490187
mms.sagepub.com

SAGE

Kinetics of a twinning step

Lifeng Liu, Anna Vainchtein and YangYang Wang
Department of Mathematics, University of Pittsburgh, Pittsburgh, USA

Received 13 March 2013; accepted 23 April 2013

Abstract
We study the kinetics of a step propagating along a twin boundary in a cubic lattice undergoing an antiplane shear deformation. To model twinning, we consider a piecewise quadratic double-well interaction potential with respect to one component of the shear strain and harmonic interaction with respect to another. We construct semi-analytical traveling wave solutions that correspond to a steady step propagation and obtain the kinetic relation between the applied stress and the velocity of the step. We show that this relation strongly depends on the width of the spinodal region where the double-well potential is non-convex and on the material anisotropy parameter. In the limiting case when the spinodal region degenerates to a point, we construct new solutions that extend the kinetic relation obtained in the earlier work of Celli, Flytzanis and Ishioka into the low-velocity regime. Numerical simulations suggest stability of some of the obtained solutions, including low-velocity step motion when the spinodal region is sufficiently wide. When the applied stress is above a certain threshold, nucleation and steady propagation of multiple steps are observed.

Keywords
Kinetic relation, twinning step, lattice model, radiative damping, spinodal region

1. Introduction

Deformation twinning is a phenomenon observed in many metals and alloys. A twin boundary separates two adjacent regions of a crystal lattice that are related to one another by simple shear. Martensites, in particular, are known to form twinning microstructures under mechanical deformation [1]. Formation and motion of twin boundaries are responsible for the ability of these materials to accommodate very large deformations (up to 8–10% strain). A twin boundary propagates forward via the motion of steps, or ledges, along it [2–5]. Lattice dynamics of steps thus largely determines the macroscopic kinetics of a twin boundary [6, 7].

In this work we study the kinetics of a single step propagating along the twin boundary. To model this phenomenon in the simplest setting, we consider antiplane shear deformation of a cubic lattice, with piecewise quadratic double-well interaction potential with respect to one component of the shear strain and harmonic interaction with respect to another. The two wells represent two different twin variants and are separated by a *spinodal* region where the potential is non-convex. This is an extension of the model with bilinear interactions that was used in [8, 9] to study high-velocity dynamics of steps along a phase boundary and in [10], where their quasistatic evolution was considered. Piecewise linear interactions were assumed by many authors to describe propagation of phase boundaries, fracture and dislocations in a crystal lattice (see [11–24] and references therein). The advantage of such models is that they allow a semi-analytical treatment through the application of Fourier transform, Wiener–Hopf technique and related methods.

Corresponding author:
Anna Vainchtein, Department of Mathematics, University of Pittsburgh, Pittsburgh, PA 15260, USA.
Email: aav4@pitt.edu

To find the kinetic relation between the applied stress and the velocity of the step, we need to construct traveling wave solutions representing the steady motion of a twinning step. The problem trivially reduces to the uniform motion of a screw dislocation studied in [15] (see also [25, 26]), where it is shown that semi-analytical solutions can be obtained by solving a linear integral equation. The kernel of the integral equation is determined by the solution of the problem where spinodal region degenerates into a point, which was studied in [13, 16]; see also [11] for a closely related one-dimensional Frenkel–Kontorova (FK) model. Despite the long history of this problem, some important questions remained open. One of these questions is the existence and stability of the low-velocity motion. In fact, the work in [15, 25, 26] focused primarily on solutions at some fixed velocities in the medium to high range and their dependence on the width of the spinodal region, while the slow propagation was not investigated. Here we use the approach in [15] to construct solutions for a wide range of velocities, including slow motion, and obtain the associated kinetic relation. We show that this relation strongly depends on the width of the spinodal region and the material anisotropy parameter given by the relative strength of the harmonic bonds. We then conduct numerical simulations to independently verify some of these results and test stability of the obtained solutions. We provide semi-analytical and numerical evidence that not only steady slow dislocation (step) motion exists, it may become stable when the spinodal region is sufficiently wide. Unlike the high-velocity motion, a slowly moving step requires very small stress and emits lattice waves that may propagate both behind and ahead of the moving front. Our work thus complements and extends the results in [15, 25, 26]. It also extends to the higher-dimensional case the work in [23], where a similar investigation was recently undertaken for the FK model.

We also revisit the limiting case when the spinodal region between the two wells degenerates into a single point (spinodal value). In this case the earlier work [13, 16] considered traveling wave solutions in which a transforming bond goes through the spinodal value at a single transition point, which means that it *instantaneously* switches from one well to another and remains there. While this assumption seems reasonable, it generates solutions only at relatively high velocities above a certain threshold value V_0 (and below another critical velocity where the solutions break down). Below V_0, the formally constructed solutions violate the assumption used to obtain them because the transforming bond crosses the spinodal value more than once. This implies that no traveling wave solutions of the form assumed in [13, 16] exist below the threshold value. The same non-existence result has been observed for the FK model [11, 17]. Meanwhile, the results obtained for the models with a non-degenerate spinodal region, both the one studied here and its FK counterpart in [23], suggest that at velocities below V_0 the time interval during which a transforming bond remains in the spinodal region approaches a *non-zero* value as the spinodal region shrinks to a point. This motivated the work [27] for the FK model, where a new type of solutions below the threshold velocity was recently constructed by extending the approach developed in [15] to this limiting case and allowing the transforming bonds to stay at the spinodal value for a *finite* time before switching into another well. Here we apply this idea to the present model and show that the same result holds. The new solutions fill in the low-velocity gap in the kinetic relation left by the analysis in [13, 16], although, as in [27], they are likely unstable.

Finally, we investigate the solution breakdown at sufficiently high velocities when the amplitude of the lattice waves emitted by a moving step becomes sufficiently large and leads to cascade nucleation, growth and coalescence of islands on top of the existing step. The boundaries of the new islands and the initial step eventually propagate with the same velocity. These results extend the analysis in [9] to the case with a non-degenerate spinodal region, where the island nucleation is no longer instantaneous, and support the dynamic twin nucleation and growth mechanism that was predicted in [28] and studied numerically in [29, 30].

The paper is organized as follows. Section 2 introduces the model, and the solution procedure is summarized in Section 3. In Section 4 we discuss the admissibility of solutions, obtain the kinetic relation and analyze its dependence on the width of the spinodal region and the material anisotropy parameter. The new solutions for the case of the degenerate spinodal region are obtained and discussed in Section 5. In Section 6 we numerically investigate stability of the obtained solutions, and some concluding remarks can be found in Section 7. Some additional technical results are contained in Appendices A and B.

2. The model

Consider a three-dimensional cubic lattice with an orthonormal basis $\{\mathbf{e_1}, \mathbf{e_2}, \mathbf{e_3}\}$ undergoing an antiplane shear deformation, which means that the atomic rows parallel to the $\mathbf{e_3}$-direction are rigid and can only move along their length. Let $u_{m,n}(t)$ denote the displacement of (m, n)th row at time t. We assume that each row interacts with its four nearest neighbors. The interaction potentials between the neighboring rows in the horizontal (m)

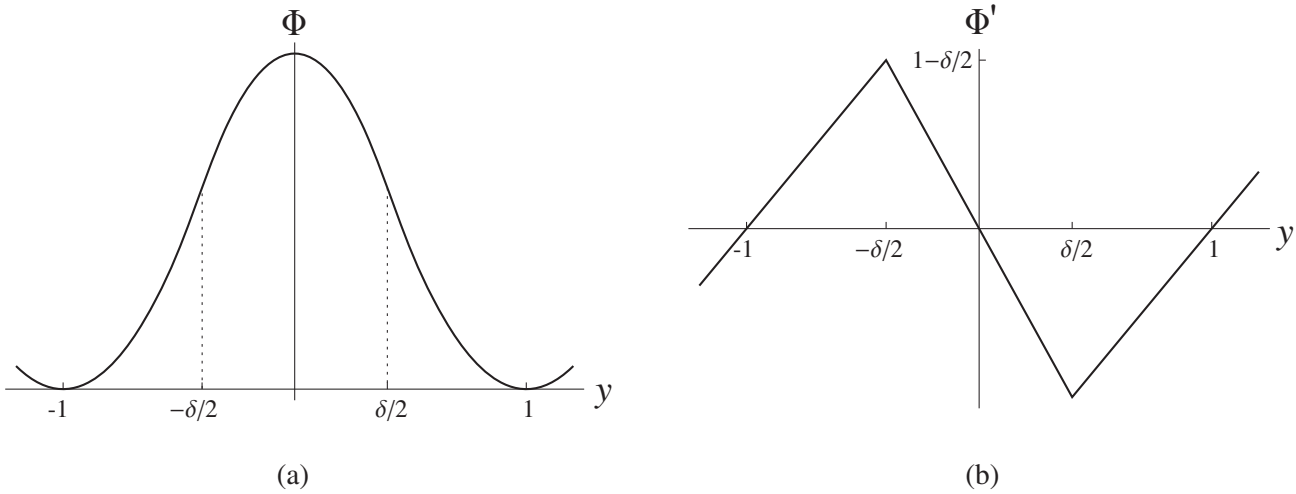

Figure 1. The double-well quadratic potential $\Phi(y)$ and its derivative (2).

and vertical (n) directions are given by $\Psi(e)$ and $\Phi(y)$, where e and y denote the corresponding components of the shear strain. The equations of motion are then given by the infinite system of ordinary differential equations:

$$\begin{aligned}\frac{d^2}{dt^2}u_{m,n}(t) = {} & \Psi'(u_{m+1,n}(t) - u_{m,n}(t)) - \Psi'(u_{m,n}(t) - u_{m-1,n}(t)) \\ & + \Phi'(u_{m,n+1}(t) - u_{m,n}(t)) - \Phi'(u_{m,n}(t) - u_{m,n-1}(t)).\end{aligned} \tag{1}$$

Here all variables are dimensionless after an appropriate rescaling [8].

To model twinning, we assume that the bonds in the vertical direction are governed by a double-well potential, with a continuous *trilinear* derivative:

$$\Phi'(y) = \begin{cases} y+1, & y < -\delta/2 \quad \text{(variant I)}, \\ (1-2/\delta)y, & |y| \le \delta/2 \quad \text{(spinodal region)}, \\ y-1, & y > \delta/2 \quad \text{(variant II)}. \end{cases} \tag{2}$$

The two symmetric quadratic wells of $\Phi(y)$ correspond to two different twin variants I and II and are connected by a downward parabola that represents the spinodal region of width δ such that $0 < \delta < 2$ (see Figure 1). In what follows, we will also separately consider the limiting case $\delta = 0$ when the spinodal region degenerates to a single point, and $\Phi'(y)$ becomes *bilinear*, $\Phi'(y) = y \pm 1, y \lessgtr 0$. We further assume that the elastic interactions between the nearest neighbors in the horizontal bonds are linear:

$$\Psi'(e) = \chi e. \tag{3}$$

Here $\chi > 0$ is the dimensionless parameter measuring the anisotropy of the lattice. We note that while in general the interaction potentials are periodic, with alternating slip and twinning energy barriers, here we assume that the energy barrier for twinning is much lower than the one for slip, as is the case, for example, in Cu–Al–Ni alloy [6], so it suffices to consider only two wells. On the continuum level, constitutive laws similar to the one assumed here were used to model twinning in [31, 32].

Suppose now that a twin boundary containing a single step divides the lattice into two regions, as shown in Figure 2. The vertical bonds in the blue region are in variant II, the bonds in the red region are in variant I, and there are possibly also some bonds near the step front that have spinodal strain values (the green region). As the step propagates from left to right along the twin boundary, the spinodal (green) bonds switch to variant II (blue), and the variant I (red) bonds switch to the spinodal region (green) and later to variant II. In what follows, we will consider traveling wave solutions describing a steady step propagation and obtain the corresponding *kinetic relations* between the applied stress and the velocity of the step.

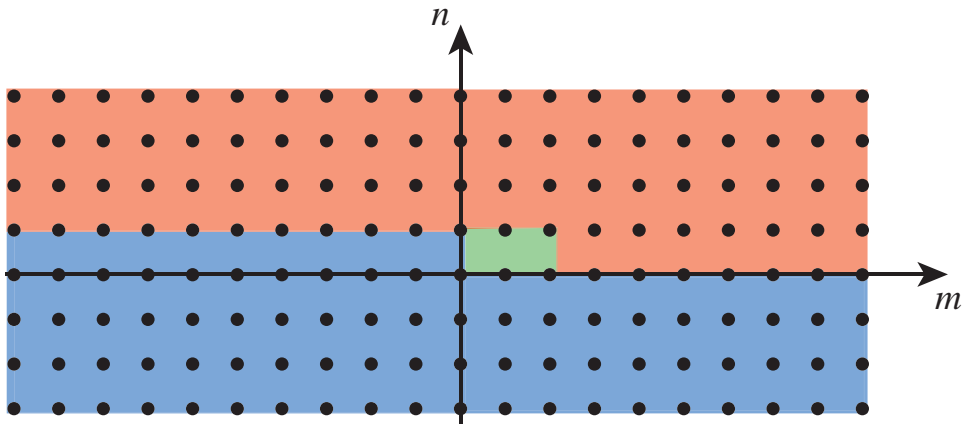

Figure 2. A twin boundary with a single step. Vertical bonds inside the blue region are in variant II, bonds in the red region are in variant I, and the strains of the vertical bonds inside the green region have spinodal values.

3. Traveling wave solution

To model a steadily moving step front along the twin boundary, we seek solutions of (1) in the form of a traveling wave with (constant) velocity $V > 0$:

$$u_{m,n}(t) = u(\xi, n), \quad \xi = m - Vt. \tag{4}$$

The vertical strains $y_{m,n}(t) = u_{m,n}(t) - u_{m,n-1}(t)$ are then given by

$$y_{m,n}(t) = y(\xi, n) = u(\xi, n) - u(\xi, n-1).$$

We assume that at infinity the vertical strain tends to constant values $y_+ < 0$ and $y_- > 0$ in variant I and variant II, respectively:

$$\begin{aligned} &y(\xi, n) \to y_\pm, \quad \text{as } n \to \pm\infty \\ &y(\xi, n) \to \begin{cases} y_+, & n \geq 2 \\ y_\pm, & n = 1 \\ y_-, & n \leq 0, \end{cases} \quad \text{as } \xi \to \pm\infty. \end{aligned} \tag{5}$$

Furthermore, we assume the horizontal strains vanish at infinity:

$$e_{m,n}(t) = u_{m,n}(t) - u_{m-1,n}(t) \to 0, \quad \text{as} \quad m^2 + n^2 \to \infty.$$

Note that under these assumptions the 31 component of the shear stress tends to zero at infinity, and in view of (2), the applied shear stress $\sigma_{32} = \sigma$ is given by $\sigma = y_+ + 1 = y_- - 1$, so that

$$y_\pm = \sigma \mp 1. \tag{6}$$

Observe also that the displacement $u_{m,n}(t)$ is determined up to an additive constant which can be fixed by specifying displacement of a lattice point. As illustrated in Figure 2, we assume that the vertical bonds at $n \geq 2$ and $n \leq 0$ remain in their respective variants:

$$y(\xi, n) < -\delta/2, \quad n \geq 2 \quad \text{(variant I)}, \qquad y(\xi, n) > \delta/2, \quad n \leq 0 \quad \text{(variant II)}. \tag{7}$$

Meanwhile, the vertical bonds at $n = 1$ can switch from the first to second variant as the step propagates to the right by going through the spinodal region. Following the approach used in [15], we assume that $y(\xi, 1)$ takes

values inside the spinodal region when $|\xi| < z$, for some $z > 0$ to be determined, and is in the corresponding variant outside this interval:

$$\begin{aligned} y(\xi,1) &< -\frac{\delta}{2}, \quad \xi > z \quad \text{(variant I)},\\ |y(\xi,1)| &< \frac{\delta}{2}, \quad |\xi| < z \quad \text{(spinodal region)},\\ y(\xi,1) &> \frac{\delta}{2}, \quad \xi < -z \quad \text{(variant II)}, \end{aligned} \tag{8}$$

and the switch between variant I (II) and the spinodal region takes place at $\xi = \pm z$:

$$y(z,1) = -\frac{\delta}{2}, \quad y(-z,1) = \frac{\delta}{2}. \tag{9}$$

Under the above assumptions we can write

$$\Phi'(y(\xi,1)) = y(\xi,1) + 1 - 2\int_{-z}^{z} \theta(s-\xi)h(s)\,ds, \tag{10}$$

where $\theta(s)$ is a unit step function: $\theta(s) = 1$ for $s > 0$; $\theta(s) = 0$ for $s < 0$. Here we have introduced an unknown shape function $h(s)$, which is zero outside the interval $[-z, z]$ and is normalized so that

$$\int_{-z}^{z} h(s)\,ds = 1. \tag{11}$$

Using (4), (10) and the assumed inequalities (7) and (8), we rewrite the equations of motion (1) as

$$\begin{aligned} V^2\frac{\partial^2}{\partial\xi^2}u(\xi,n) =& \chi\left(u(\xi+1,n) + u(\xi-1,n) - 2u(\xi,n)\right) + u(\xi,n+1) + u(\xi,n-1)\\ &-2u(\xi,n) + 2\left[\delta_{n,0} + (\delta_{n,1} - \delta_{n,0})\int_{-z}^{z} h(s)\theta(s-\xi)\,ds\right]. \end{aligned} \tag{12}$$

The solution of (12) can be represented as the sum of the solution of the static problem with a flat twin boundary along $n = 0$ at zero stress and a solution of the dynamic problem for a screw dislocation located at the step front and moving steadily under the applied stress. More precisely, we write

$$u(\xi,n) = u_n^F + w(\xi,n), \tag{13}$$

where

$$u_n^F = \begin{cases} 0, & n \geq 0\\ 2n, & n \leq -1 \end{cases} \tag{14}$$

satisfies the static flat-boundary problem

$$u_{n+1}^F + u_{n-1}^F - 2u_n^F + 2\delta_{n,0} = 0, \tag{15}$$

and the screw dislocation solution is given, up to an additive constant, by [15]

$$w(\xi,n) = n(\sigma - 1) + \frac{1}{2\pi^2}\int_{-\infty}^{\infty} \frac{e^{-ik_\xi\xi}H(k_\xi)\mathcal{J}(k_\xi,n)}{i(k_\xi - i0)}\,dk_\xi. \tag{16}$$

Here $k_\xi - i0 = \lim_{\varepsilon\to 0+}(k_\xi - i\varepsilon)$, $H(k_\xi)$ is the Fourier transform of $h(\xi)$ and

$$\mathcal{J}(k_\xi,n) = \int_{-\pi}^{\pi} \frac{(1-e^{i\kappa})e^{-in\kappa}}{V^2k_\xi^2 - 4(\chi\sin^2\frac{k_\xi}{2} + \sin^2\frac{\kappa}{2})}\,d\kappa \tag{17}$$

is defined for integer n. The integral in (17) can be explicitly calculated using the residue theorem, yielding (41) in Appendix A. Using (13), (14), (16) and the convolution properties of the Fourier transform, we obtain the vertical strains in the lattice as

$$y(\xi,n)=\int_{-z}^{z} g_{|n-1|}(\xi-s)h(s)\,ds+\begin{cases}\sigma-1, & n\geq 1,\\ \sigma+1, & n\leq 0.\end{cases} \tag{18}$$

Here we defined

$$g_j(\xi)=\frac{1}{\pi}\int_{-\infty}^{\infty}\frac{e^{-ik_\xi\xi}}{i(k_\xi-i0)}\mathcal{S}(k_\xi,j)\,dk_\xi,\quad j=0,1,2,\ldots, \tag{19}$$

where

$$\mathcal{S}(k_\xi,j)=\begin{cases}(\lambda-\sqrt{\lambda^2-1})^{-|j|}(\delta_{j,0}-\sqrt{\frac{\lambda-1}{\lambda+1}}), & \lambda<-1\\ (\lambda\mp i\sqrt{1-\lambda^2})^{-|j|}(\delta_{j,0}\pm i\sqrt{\frac{1-\lambda}{1+\lambda}}), & |\lambda|<1,\quad k_\xi\lessgtr 0\\ (\lambda+\sqrt{\lambda^2-1})^{-|j|}(\delta_{j,0}-\sqrt{\frac{\lambda-1}{\lambda+1}}), & \lambda>1\end{cases} \tag{20}$$

and

$$\lambda(k_\xi)=1+2\chi\sin^2\frac{k_\xi}{2}-\frac{1}{2}V^2k_\xi^2. \tag{21}$$

Observe now that on one hand, we have

$$\frac{\partial}{\partial\xi}y(\xi,1)=-\int_{-z}^{z}q(\xi-s)h(s)\,ds, \tag{22}$$

where, by (18) and (19),

$$q(\xi)=-g_0'(\xi)=\frac{1}{\pi}\int_{-\infty}^{\infty}e^{-ik_\xi\xi}\mathcal{S}(k_\xi,0)\,dk_\xi. \tag{23}$$

On the other hand, (2) and (10) imply that for $|\xi|<z$

$$y(\xi,1)=\delta\left(\int_{\xi}^{z}h(s)ds-\frac{1}{2}\right),$$

and thus

$$\frac{\partial}{\partial\xi}y(\xi,1)=-\delta h(\xi). \tag{24}$$

Together, (22) and (24) yield a Fredholm integral equation of the second kind [15]:

$$\int_{-z}^{z}q(\xi-s)h(s)\,ds=\delta h(\xi),\quad |\xi|<z, \tag{25}$$

where the shape function $h(\xi)$ is an eigenfunction of the integral operator in the left-hand side of (25) with kernel (23) associated with the eigenvalue δ. The problem thus reduces to solving the integral equation (25) for z and $h(\xi)$.

Once $h(\xi)$ and z are known, the vertical strains for the traveling wave solution can be computed from (18). Substituting (18) into the switch conditions (9) and subtracting the first condition from the second, we obtain $\int_{-z}^{z}(g_0(-z-s)-g_0(z-s))h(s)\,ds=\delta$, which is automatically satisfied, as can be verified by integrating (25) and recalling (11) and the first equality in (23). Meanwhile, adding the two conditions yields the following expression for the applied stress:

$$\sigma=1-\frac{1}{2}\int_{-z}^{z}h(s)[g_0(z-s)+g_0(-z-s)]\,ds. \tag{26}$$

Since g_0 depends on V, this defined the *kinetic relation* $\sigma=\Sigma(V)$ between the applied stress σ and the step moving velocity V. The relation also depends on δ and χ.

We remark that the real wave numbers k_ξ such that $|\lambda(k_\xi)| \leq 1$, with λ given by (21), correspond to the *lattice waves* emitted by the moving step because this inequality implies the existence of real wave numbers κ such that the velocity of the moving step equals the horizontal component of the phase velocity of some plane waves: $V = \omega/k_\xi$, where $\omega^2 = 4(\chi \sin^2(k_\xi/2) + \sin^2(\kappa/2))$ is the dispersion relation [13]. One can show [15] that only these waves, which carry energy away from the step, contribute to the stress in (26). The transfer of energy from long (continuum level) to short (lattice-scale) waves associated with this nonlinearity-induced radiation is known in the physics literature as the radiative damping phenomenon (e.g. [17]). Analyzing the asymptotic strain behavior as in [8, 15, 33], one can show that the amplitude of the lattice waves slowly decays as $|\xi|$ increases, so that the strains tend to constant values at infinity, as assumed in (5).

It should be emphasized that the solutions of (12) satisfy the original nonlinear equation (1) if and only if the *admissibility conditions* (7) and (8) hold. Solutions of (12) that violate any of the admissibility conditions will be called *inadmissible*.

4. Admissible solutions and kinetic relations

We first review the limiting case $z = 0$ that reduces to the screw dislocation problem studied in [15, 16]. One can see that in this limit we must have $\delta = 0$, i.e. spinodal region degenerates to a single point and $\Phi'(y)$ becomes bilinear, while the shape function becomes a Dirac delta function: $h(s) = \delta_D(s)$. Thus, Equation (18) reduces to

$$y^0(\xi, n) = u^0(\xi, n) - u^0(\xi, n-1) = g_{|n-1|}(\xi) + \begin{cases} \sigma - 1, & n \geq 1, \\ \sigma + 1, & n \leq 0, \end{cases} \tag{27}$$

where $u^0(\xi, n)$ satisfies

$$\begin{aligned} V^2 \frac{\partial^2}{\partial \xi^2} u^0(\xi, n) =& \chi(u^0(\xi+1, n) + u^0(\xi-1, n) - 2u^0(\xi, n)) + u^0(\xi, n+1) + u^0(\xi, n-1) \\ & - 2u^0(\xi, n) + 2\left[\delta_{n,0} + (\delta_{n,1} - \delta_{n,0})\theta(-\xi)\right]. \end{aligned} \tag{28}$$

We observe that the first equality in (23) and (27) imply that

$$q(\xi) = -\frac{\partial y^0(\xi, 1)}{\partial \xi}. \tag{29}$$

Note that the vertical strain $y^0(\xi, n)$ should also satisfy the corresponding admissibility conditions (7) and (8) at $z = 0$ and $\delta = 0$, which reduce to (with $y = y^0$)

$$y(\xi, n) < 0, \quad n \geq 2 \quad \text{(variant I)}, \qquad y(\xi, n) > 0, \quad n \leq 0 \quad \text{(variant II)}. \tag{30}$$

and

$$y(\xi, 1) < 0, \quad \xi > 0 \quad \text{(variant I)}, \qquad y(\xi, 1) > 0, \quad \xi < 0 \quad \text{(variant II)}, \tag{31}$$

respectively. The kinetic relation (26) can be shown in this case to yield $\sigma = \Sigma_0(V)$ defined by

$$\sigma = 1 - g_0(0) = \frac{2}{\pi} \int_0^\infty \frac{1}{k_\xi} \sqrt{\frac{1 - \lambda(k_\xi)}{1 + \lambda(k_\xi)}} \theta(1 - |\lambda(k_\xi)|)\, dk_\xi, \tag{32}$$

where we recall that $\lambda(k_\xi)$ is given by (21). The reader is referred to [8, 13, 16] for more details.

The resulting kinetic relation, shown in Figure 3(a), consists of disjoint segments separated by *resonance velocities*, i.e. values of V such that $\lambda(k_\xi) = -1$ and $\lambda'(k_\xi) = 0$ for some real k_ξ (see Figure 3(b)). At these velocities the kinetic relation has either a logarithmic singularity (at the resonance velocities that correspond to the local minima of $V(k_\xi)$ such that $\lambda = -1$) or a jump discontinuity (at the local maxima) [16]. A typical admissible solution ($V = 0.5$) above the first resonance $V_1 \approx 0.3158$ is shown in Figure 4(a). One can see that the moving step generates lattice waves behind it. As velocity decreases below the first resonance, solution develops oscillations at $\xi > 0$ as well; see, for example, the vertical strain profile at $V = 0.17$ in Figure 4(b),

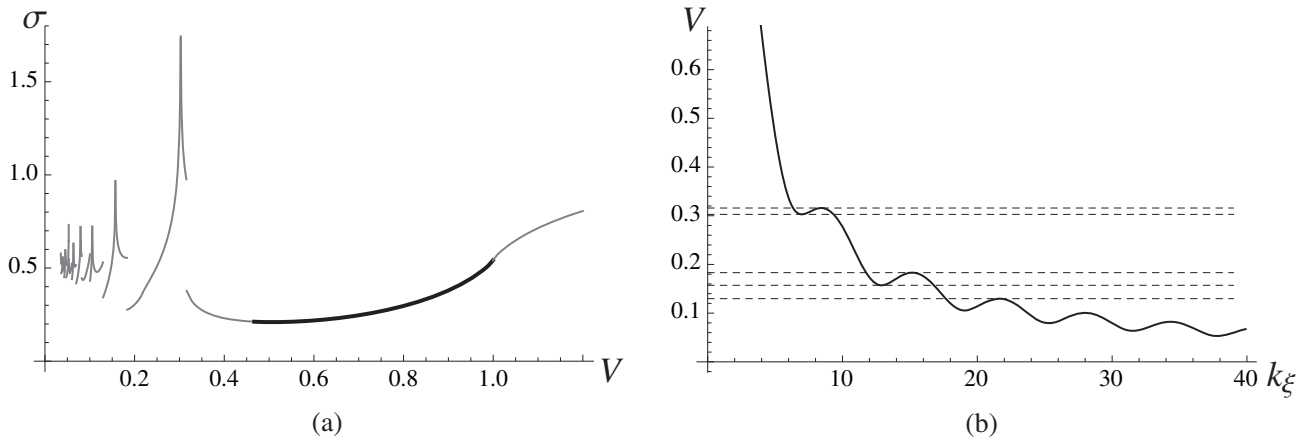

Figure 3. (a) Kinetic relation $\sigma = \Sigma_0(V)$ at $z = 0$, $\delta = 0$. Only the first 20 segments are shown. Admissible solutions correspond to the dark portion of the first segment. (b) Velocities V such that $\lambda = -1$ for positive real k_ξ. The dashed lines indicate the first five resonance velocities at which $\lambda(k_\xi) = -1$ and $\lambda'(k_\xi) = 0$. Here $\chi = 1$.

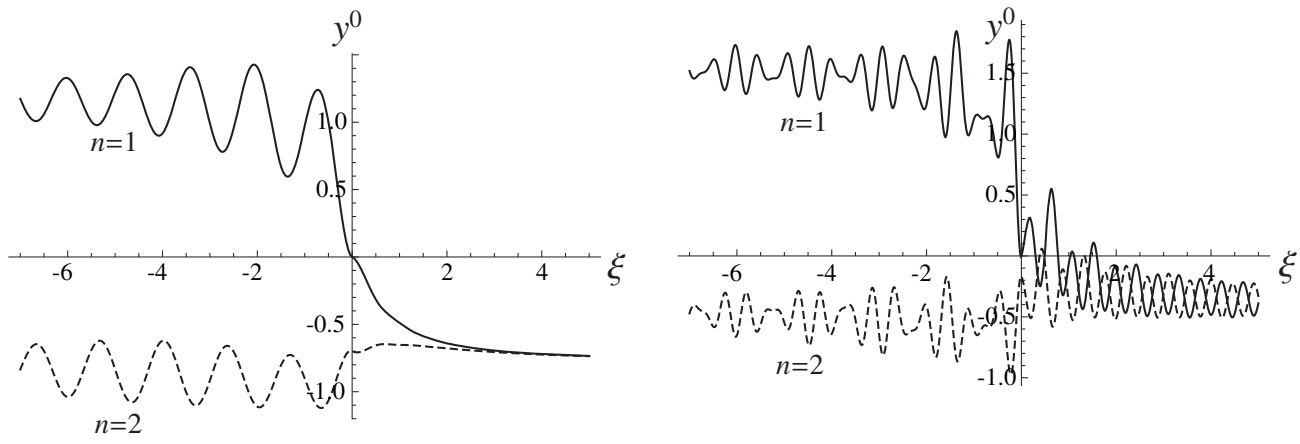

Figure 4. Vertical strain $y^0(\xi, n)$ profiles at $n = 1, 2$ formally computed from (27) and (32) at $z = 0$, $\delta = 0$, $\chi = 1$ and velocities (a) $V = 0.5$ ($\sigma = 0.2096$) and (b) $V = 0.17$ ($\sigma = 0.5736$). The solution in (a) satisfies the constraints (30) and (31) but the solution in (b) violates both constraints at $\xi > 0$. Here and in the following figures, $n = 0$ strains are not shown because by the symmetry of $g_{|n-1|}(\xi)$ and (18), $y(\xi, 0) = y(\xi, 2) + 2$.

where two modes of emitted lattice waves propagate behind and one mode ahead of the step. However, a closer inspection reveals that this solution is in fact *inadmissible* and should be removed because it violates the first inequality in both (30) and (31). At $\chi = 1$, our calculations show that the large-velocity segment contains admissible solutions above a certain threshold, $V \geq V_0 \approx 0.4649$, while in several segments of the kinetic relation below the threshold, we only found inadmissible traveling waves that violate (31) and sometimes also (30), and thus need to be removed. This suggests non-existence of traveling wave solutions with velocity lower than the threshold value in the $z = 0$ case, in agreement with the conjectures made in [13, 16]. Meanwhile, solutions at sufficiently high velocities ($V \geq V_h \approx 0.9908$ at $\chi = 1$) are also inadmissible, because the large amplitude of waves propagating behind the step front causes the $n = 2$ bonds directly above the step to switch from variant I to variant II, which violates the first inequality in (30) (see also [8]).

Consider now the trilinear problem with $\delta > 0$. To find $h(s)$ and z for given non-resonant $V > 0$ and $\delta > 0$, we approximate the integral equation (25) by a trapezoidal rule with an uniform mesh, obtaining a homogeneous linear system $(\mathbf{Q}(z) - \delta\mathbf{I})\mathbf{h} = \mathbf{0}$, where $\mathbf{Q}(z)$ is the matrix approximating the integral operator, $\mathbf{I}$ is the identity matrix, and $\mathbf{h}$ is the vector approximating the unknown shape function. To find z, we solve the

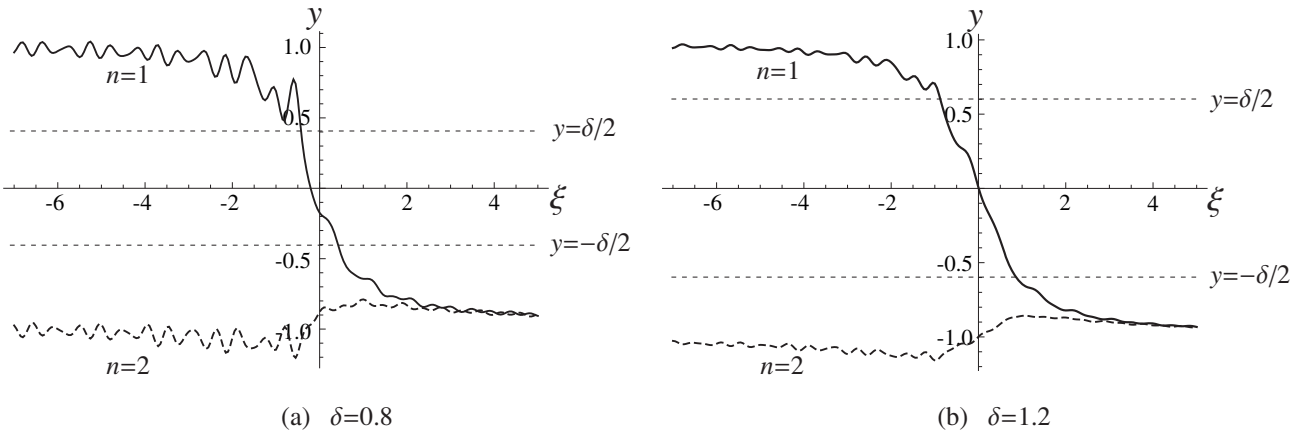

Figure 5. Vertical strain $y(\xi, n)$ ($n = 1, 2$) profiles at $V = 0.17$, with (a) $\delta = 0.8$ ($z = 0.424$, $\sigma = 0.0409$) and (b) $\delta = 1.2$ ($z = 0.875$, $\sigma = 0.0039$). Both solutions are admissible. Here $\chi = 1$.

nonlinear algebraic equation $\det(\mathbf{Q}(z) - \delta\mathbf{I}) = 0$, which ensures that δ is an eigenvalue of $\mathbf{Q}(z)$, and then find the corresponding eigenvector $\mathbf{h}$, normalized by (11). In general, there may be more than one value of z but our calculations suggest that at most one value yields admissible solutions. Once z and $\mathbf{h}$ are found, the trapezoidal approximation of the integrals in (18) and (26) is used to compute the solution $y(\xi, n)$ and the applied stress σ.

The resulting vertical strains of $n = 1$ and $n = 2$ bonds at $V = 0.17$ are shown by Figure 5 for $\delta = 0.8$ (which yields $z = 0.424$ and $\sigma = 0.0409$) and $\delta = 1.2$ ($z = 0.875$ and $\sigma = 0.0039$). As in [15], we observe that the main effect of increasing δ, which leads to larger z, is the decreased amplitude of the oscillations due to wave modulation that takes place over the larger time interval. As a result, the solutions at $V = 0.17$ become admissible at $\delta = 0.8$ and $\delta = 1.2$, while the corresponding solution of the bilinear problem at $z = 0$ is not. Note also that the stress decreases as δ is increased due to the smaller contribution of the lattice waves, although it may oscillate at larger values of δ (see [25, 26]).

Figure 6 shows the half-width z of the transition region as a function of V for different δ at $\chi = 1$, and the corresponding kinetic relations are shown in Figure 7. Due to the pile-up of resonance velocities as V approaches zero, which makes the computation progressively more difficult, only $V \geq 0.1$ were considered. A detailed inspection suggests that all solutions shown except those along the gray portions of the curves are admissible. This includes solutions in the immediate vicinity of the resonance velocities, which correspond to the cusps in Figures 6 and 7. Note that the kinetic relations are highly non-monotone, with larger stress variations at lower δ. Observe also that at $\delta = 1.2$ the low-velocity motion requires very little applied stress, due to the small amplitude of the emitted waves and thus small amount of radiative damping. This "soliton-like" dislocation behavior is discussed in [25, 26].

Interestingly, as in [23], our numerical calculations reveal that as δ approaches zero at velocities below the threshold value $V_0 \approx 0.4649$, the value of z approaches a positive value rather than zero, in contrast to the assumption of $z = 0$ in [13, 16] for the bilinear case. This motivates us to construct a new type of traveling wave solutions for the limiting case $\delta = 0$ that has $z > 0$ below the threshold value. We postpone the discussion of these new solutions until Section 5, while here we simply show the corresponding curves for comparison.

We now consider the dependence of the kinetic relation $\sigma = \Sigma(V)$ on χ, the dimensionless anisotropy parameter measuring the shear strength of the linearly elastic horizontal bonds relative to the vertical ones. Let $c = \sqrt{\chi}$ be the sound speed of elastic shear waves in the horizontal direction of the step motion. At $\delta = 0.8$, typical kinetic relations at different χ are shown in Figure 8(b) and the corresponding $z(V)$ graphs in Figure 8(a). Note that the resonance velocities take different values for different χ, so the locations of the cusps in the kinetic relation changes. One can see that a higher χ results in a lower applied stress at the same normalized velocity V/c because it means a stronger coupling of the vertical bonds.

At sufficiently large velocities above a threshold V_h (for example, $V > V_h \approx 0.9389$ at $\delta = 0.8$ and $\chi = 1$), the amplitude of the waves propagating behind the step front becomes so large that the strain in some $n \geq 2$ bonds above the step enters the spinodal region from variant I, violating the first constraint in (7) and thus rendering the corresponding solutions inadmissible (see the gray large-velocity segments in Figures 6(a), 7(a) and 8). One can observe that at $\chi = 1$ the upper threshold V_h increases as δ decreases. Meanwhile, at the same

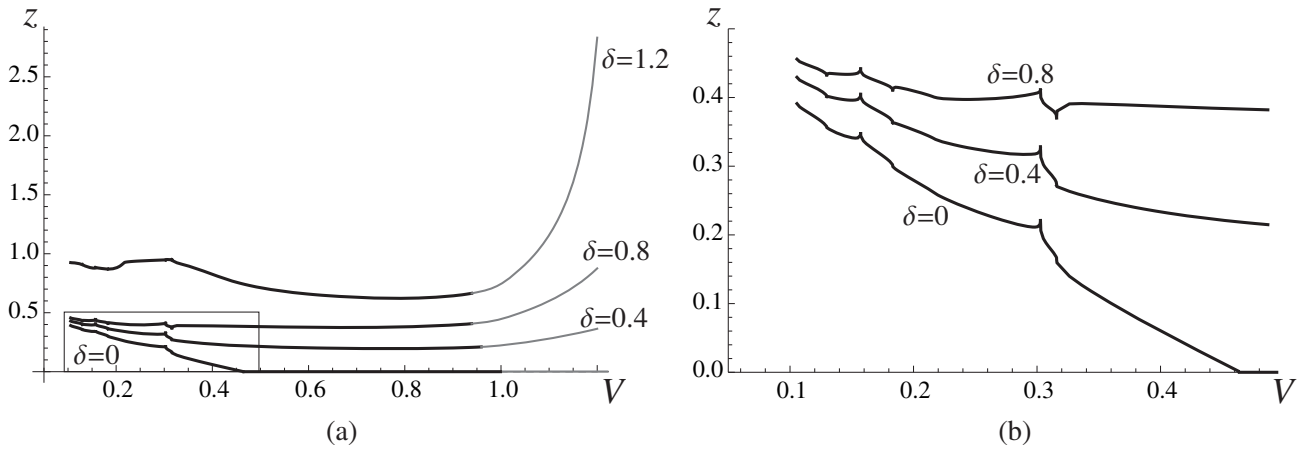

Figure 6. (a) The half-width $z(V)$ of the transition region for different δ calculated for $V \geq 0.1$. (b) Enlarged view of the small-velocity region inside the rectangle. Here $\chi = 1$. The thicker black segments contain admissible solutions, while the gray segments correspond to inadmissible solutions.

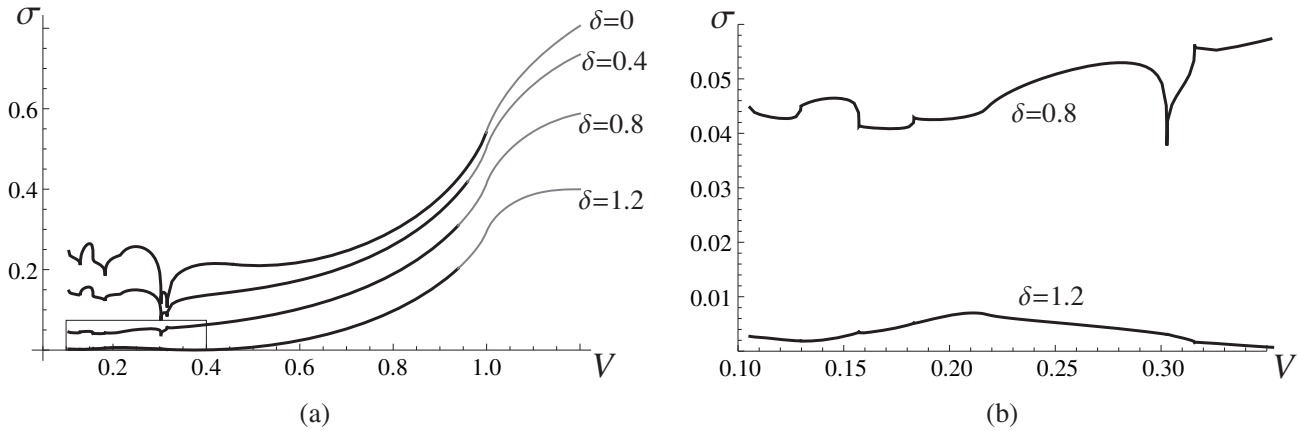

Figure 7. (a) Kinetic relations $\sigma = \Sigma(V)$ for different δ and $V \geq 0.1$. (b) Enlarged view of the small-velocity region inside the rectangle. Here $\chi = 1$. The thicker black segments contain admissible solutions, while the gray segments correspond to inadmissible solutions.

$\delta = 0.8$, the normalized upper threshold V_h/c increases as χ is increased. As we will see in Section 6, this solution failure at $\sigma > \sigma_h = \Sigma(V_h)$ corresponds to a cascade nucleation of new steps.

In addition to the traveling wave solutions, there are equilibrium states ($V = 0$) that exist when the applied stress is in the *trapping region* $|\sigma| \leq \sigma_P$, where σ_P is the Peierls stress (51). One can show [34] that at $0 < \delta < 2$ there are two equilibrium states with the assumed single-step configuration for $|\sigma| < \sigma_P$, a stable state with m_s spinodal vertical bonds near the step front and an unstable state with $m_s + 1$ spinodal bonds, where m_s and σ_P determined by δ and χ (see Appendix B for more details). These solutions are given by (46) for $m_s = 0$ and (49), (50) for $m_s \geq 1$.

5. New traveling wave solutions

We now revisit the bilinear problem ($\delta = 0$) with degenerate spinodal region, where, as we recall, no admissible solutions were found for $V < V_0$ at $z = 0$. However, as we already mentioned above, our results for small δ in this velocity region suggest that z tends to a *non-zero* value as δ approaches zero. This suggests that following the approach recently pursued for the one-dimensional problem [27], we should seek solutions with $z > 0$ and replace the admissibility conditions (31) by the more general conditions

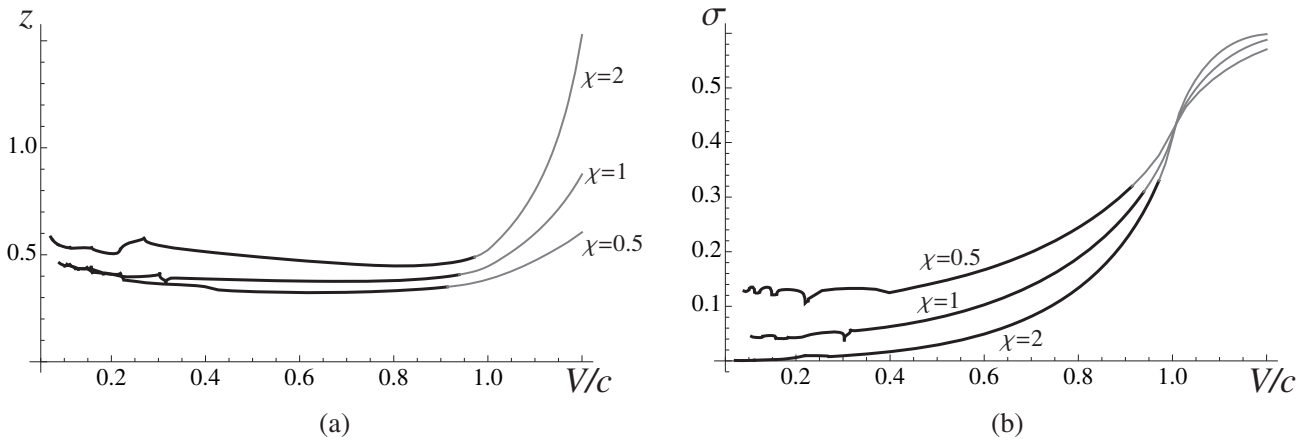

Figure 8. (a) The half-width $z(V)$ of the transition region and (b) kinetic relations $\sigma = \Sigma(V)$ at different χ. The thicker black segments contain admissible solutions, while the gray segments corresponding to inadmissible solutions. Here $\delta = 0.8$, and the velocities are normalized by $c = \sqrt{\chi}$.

$$\begin{aligned} &y(\xi,1) < 0, \quad \xi > z \quad \text{(variant I)},\\ &y(\xi,1) = 0, \quad |\xi| \le z \quad \text{(degenerate spinodal region)},\\ &y(\xi,1) > 0, \quad \xi < -z \quad \text{(variant II)}, \end{aligned} \tag{33}$$

while leaving (30) (or, equivalently, (7) at $\delta = 0$) the same. Note that (9) at $\delta = 0$ is included in (33), so we seek solutions of (12) subject to (30) and (33).

Observe now that (22) still holds. At the same time, our assumption that $y(\xi,1) \equiv 0$ at $|\xi| \le z$ implies $\frac{\partial}{\partial\xi} y(\xi,1) \equiv 0$ in the interval $(-z,z)$. Together with (22), this yields a Fredholm integral equation of the first kind:

$$\int_{-z}^{z} h(s) q(\xi - s)\, ds = 0, \quad |\xi| < z. \tag{34}$$

Thus, the shape function $h(s)$ is an eigenfunction of the integral operator in the left-hand side of (34) with kernel (23) associated with the zero eigenvalue. As before, we solve this problem numerically using the trapezoidal approximation, which now involves finding the roots of $\det\mathbf{Q}(z) = 0$, and find that at most one of these roots yields admissible solutions that satisfy (30) and (33). For example, Figure 9 shows $y(\xi,1)$ and $y(\xi,2)$ obtained at $V = 0.17$, which yields $z = 0.322$. One can see that unlike the $z = 0$ solution (the gray curves), which is inadmissible since it violates (30) and (31), the new solution (black curves) satisfies the more general admissibility condition (33) within the numerical error. We verified that it also satisfies (30) and thus is admissible. Note that like its counterparts at $\delta > 0$ at the same velocity, it involves lattice waves propagating both behind and ahead of the step.

Repeating this procedure for a range of velocities, we obtain the relation $z(V)$ between z and V at $\chi = 1$ shown in Figure 6. Note that $z(V)$ tends to zero as the velocity approaches the value $V = V_0 \approx 0.4649$. Recall that this is the threshold above which (and below $V_h \approx 0.9908$) $z = 0$ solutions of the bilinear problem become admissible. This suggests that as in [27], the new solutions with $z > 0$ bifurcate from $z = 0$ solutions at V_0. To see this, we follow the argument in [27] and consider the piecewise linear approximation of the kernel (23) in (34), as in [15]. Note that $q(\xi)$ is continuous, while $q'(\xi)$ has a jump discontinuity at $\xi = 0$, as can be shown from (29) and (28). Thus, for small ξ the kernel can be approximated by

$$\hat{q}(\xi) = \begin{cases} q_0 + q_+\xi, & \xi > 0,\\ q_0 + q_-\xi, & \xi < 0, \end{cases} \tag{35}$$

where

$$q_0 = q(0), \quad q_\pm = q'(0\pm), \quad q_+ - q_- = 4/V^2, \tag{36}$$

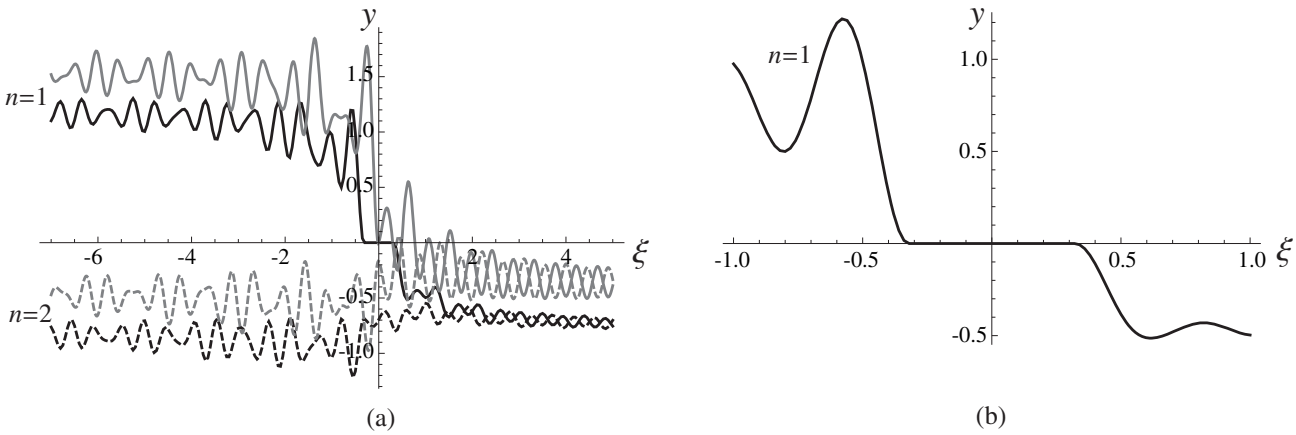

Figure 9. (a) New traveling wave solution $y(\xi, n)$ at $n = 1, 2$ and $V = 0.17$ with $z = 0.322$ (black curves), shown together with the inadmissible $z = 0$ solution $y^0(\xi, n)$ (gray curves). (b) Enlarged view of the $z = 0.322$ solution at $n = 1$. Here $\delta = 0$, $\chi = 1$ and $\sigma = 0.2139$ for the new solution.

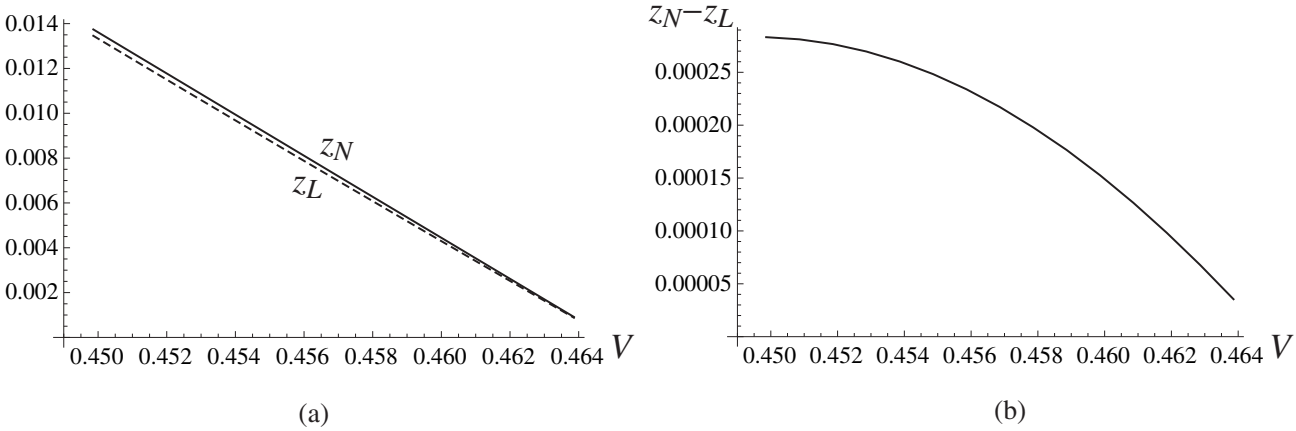

Figure 10. Comparison of the function $z_N(V)$ computed numerically using the kernel (23) (solid line) and $z_L(V)$ obtained from (37) using the linear approximation (35) of the kernel (dashed line) near the bifurcation point $V_0 \approx 0.4649$.

where the last relation is implied by (28) and (29). Solving the approximate version of (34), i.e. $\int_{-z}^{z} h(s)\hat{q}(\xi - s)ds = 0$, $|\xi| < z$, one obtains [27]

$$z = \frac{q_0(q_+ - q_-)}{2q_+q_-} \tag{37}$$

and

$$h(\xi) = \frac{q_-}{q_- - q_+}\delta_D(\xi + z) - \frac{q_+}{q_- - q_+}\delta_D(\xi - z), \tag{38}$$

in the sense of distributions. Numerical evaluation of (23) and the last of (36) show that $(q_+ - q_-)/(2q_+q_-) < 0$ when V is near the threshold V_0. Thus, the positive solution z given by (37) exists provided that $-q_0 = \frac{\partial}{\partial\xi}y^0(0, 1) > 0$. Meanwhile, the admissibility conditions (31) imply that $\frac{\partial}{\partial\xi}y^0(0, 1) \leq 0$. This indicates that bifurcation of the new type of traveling wave with $z > 0$ occurs precisely at the threshold velocity V_0, at which $q_0(V_0) = 0$, and below which the $z = 0$ solutions are inadmissible because (31) is violated. As shown in Figure 10, the values of $z(V)$ obtained from the numerical solution of (34) with the original kernel (23) near the threshold velocity V_0 approach the values (37) resulting from the linear approximation near the threshold velocity.

The corresponding kinetic relation $\sigma = \Sigma(V)$ is shown in Figure 7. It coincides with the $z = 0$ relation $\Sigma_0(V)$ above the velocity V_0, while below this threshold, where $z > 0$, it provides lower values of the applied stress and replaces the singularities in $\Sigma_0(V)$ at the resonance velocities by cusps; see Figure 11 for comparison.

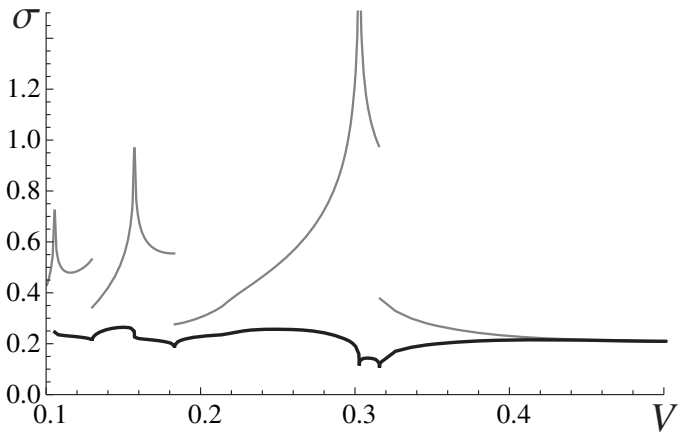

Figure 11. Comparison of the kinetic relation $\sigma = \Sigma(V)$ generated by the new solutions with $z > 0$ with the relation $\Sigma_0(V)$ obtained from the formal $z = 0$ solutions of the bilinear ($\delta = 0$) problem. The two curves coincide above the threshold velocity $V_0 \approx 0.4649$. The gray curves correspond to *inadmissible* $z = 0$ solutions below V_0.

This result thus extends the kinetic relation obtained in [13, 16] for $\delta = 0$ case into the region of velocities $V < V_0$, where the new solutions with $z > 0$ "fill the gap" left by the non-existence of admissible solutions with $z = 0$.

6. Stability of the traveling waves: numerical simulations

To investigate stability of the obtained traveling waves solutions and obtain an independent verification of our results, we solve Equations (1) numerically without assuming any particular motion pattern and then compare the numerical results with the traveling wave solutions. We use the velocity Verlet algorithm in the computational domain Ω given by a truncated 400×8 lattice. The initial configuration has a flat twin boundary with a single step in the center of the domain, as in Figure 2. To avoid reflection of lattice waves from the boundary of Ω, we use the non-reflective boundary conditions (NRBCs) developed in [9]. Assuming that the initial condition *outside* the computational domain satisfies the equilibrium equations with zero initial velocity and that the problem there remains linear (i.e. the vertical bonds remain in their respective variants), the NRBCs prescribe the displacement on $\partial\Omega^+$, a set of lattice points outside the computational domain Ω that have at least one nearest neighbor belonging to $\partial\Omega$, the boundary of Ω.

To construct the initial condition for given δ and applied stress below the Peierls threshold, $0 < \sigma < \sigma_P$, we start with an equilibrium state (stable or unstable), given by (46) if there are no spinodal bonds and (49), (50) if there is at least one such bond. To trigger step propagation, we perturb this state by changing the vertical strain in front of the step. Above the Peierls threshold, no equilibrium state exists but we use the same formulas to ensure that the initial state satisfies the equilibrium equations outside Ω, as required by the NRBCs we use. Inside the computational domain, this yields a non-equilibrium displacement. If it does not satisfy the assumed initial phase distribution, we modify the initial displacement in Ω by prescribing strains in some vertical bonds and solving a constrained equilibrium problem that ensures the assumed inequalities hold. Initial velocities are set to zero.

We find that for sufficiently small σ below the Peierls threshold the numerical solution gets trapped in a stable equilibrium state. For higher applied stress, the step propagates, and after some transient time its motion becomes steady, which means that the time period during which the front moved from one vertical bond in the lattice to the next approaches a constant value T. The velocity is then obtained by computing $V = 1/T$ as the average over the last 10 periods.

Figures 12 and 13 compare (V, σ) obtained from the numerical results (circles) for $\delta = 1.2$ and $\delta = 0.8$ (at $\chi = 1$) with the corresponding semi-analytical kinetic relation curves. One can see that the numerical results are in very good agreement with some increasing portions of the kinetic curves, which suggests stability of the traveling wave solutions with the corresponding velocities.

The fact that the numerical results only fall on the increasing portions of the curves supports the conjecture in [23] that $\Sigma'(V) > 0$ is necessary but not sufficient for stability. Note, in particular, that the results indicate

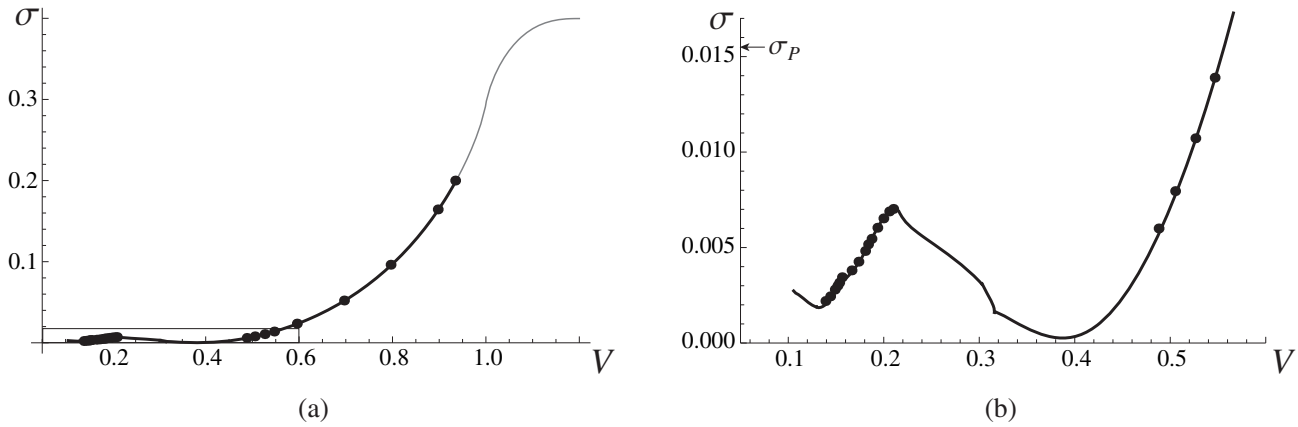

Figure 12. (a) Results of the numerical simulations for $\delta = 1.2$ (circles), shown together with the kinetic curve. (b) Enlarged view of the small-velocity region inside the rectangle in (a).

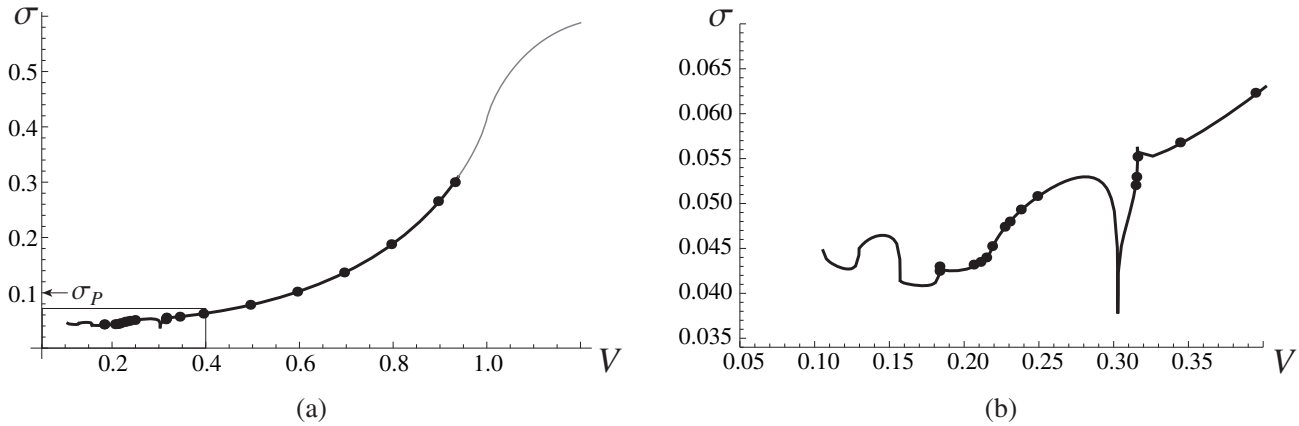

Figure 13. (a) Results of the numerical simulations for $\delta = 0.8$ (circles), shown together with the kinetic curve. (b) Enlarged view of the small-velocity region inside the rectangle in (a) (below the Peierls stress).

stability of an entire range of low-velocity motion ($0.139 \leq V \leq 0.21$) at $\delta = 1.2$ at very small values of the applied stress where the solutions coexist with stable equilibrium states. Observe also that stable solutions with different velocities may coexist at the same value of σ. For example, at $\delta = 1.2$, numerical simulations at $\sigma = 0.006$ yield steady motion at either $V = 0.193$ or $V = 0.488$, depending on the perturbation introduced in the initial conditions. Low-velocity solutions appear to be stable only when δ is sufficiently high. Meanwhile, at small δ our results indicate stability of only relatively fast traveling waves. In particular, we did not find any numerical evidence that the new traveling wave solutions constructed in Section 5 for $\delta = 0$ are stable.

As discussed in Section 4, when the applied stress is above a certain critical value $\sigma_h = \Sigma(V_h)$, which depends on δ and χ, the traveling wave solutions become inadmissible because the large-amplitude lattice waves emitted by the moving step force some vertical bonds above the step ($n \geq 2$) to have strain values outside variant I and hence violate the first inequality in (7). Our numerical simulations reveal that at the applied stress $\sigma > \sigma_h$, nucleation of new islands of variant II takes place on top of the existing step configuration. For example, at $\delta = 0.8$ and $\chi = 1$ we have $\sigma_h \approx 0.309$, and at $\sigma = 0.45$ above this threshold, after some transient time, an initial single step propagates steadily with velocity $V \approx 1.01$. This can be seen in Figure 14(a), which shows the evolution in time of the step front positions $x_n(t)$, defined by $x_n(t) = m$, where m is such that $y_{m,n}(t) > \delta/2$ and $y_{m+1,n}(t) \leq \delta/2$ for the initial step, $n = 1$.

Eventually, however, a vertical bond above the step enters the spinodal region, nucleating a new island that starts propagating on top of the initial step. For example, at $t = 12$ in Figure 15 one can see six vertical bonds that have strains in either spinodal region (green) or variant II (blue). As this island grows, its boundaries soon attain the same velocity as the initial step, as can be seen in Figure 14(a) ($n = 2$). Later on, more islands

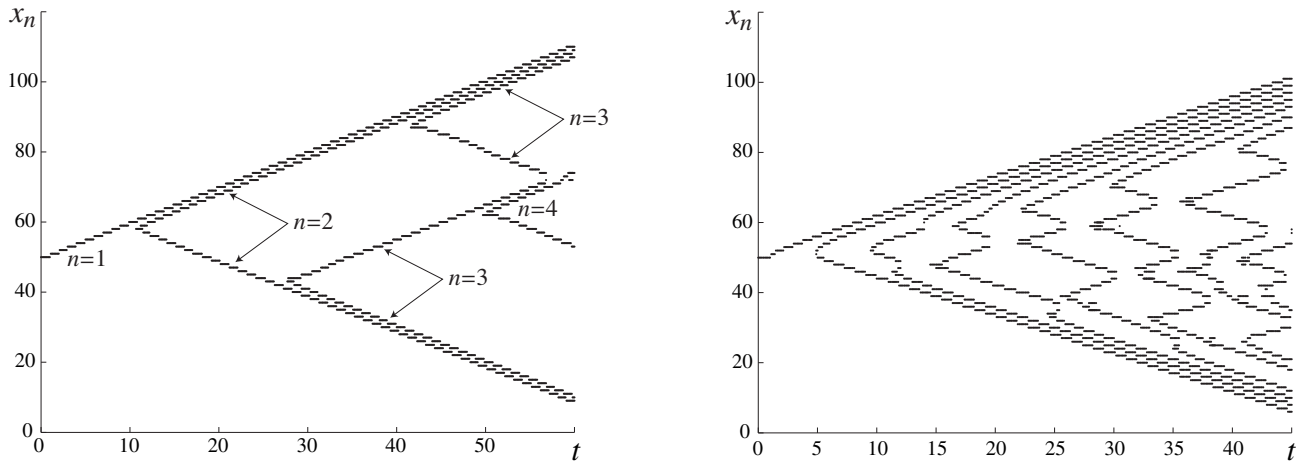

Figure 14. Evolution of step front positions $x_n(t)$ during island nucleation, propagation and coalescence at different values of the applied stress above the threshold value σ_h. Here $\delta = 0.8$ and $\chi = 1$.

nucleate, grow and coalesce, and all the fronts eventually propagate with the same velocity; see Figures 14(a) and 15. At higher applied stress, $\sigma = 0.55$, island nucleation occurs sooner, and new islands nucleate and merge more frequently (see Figure 14(b)). While these observations are similar to the results obtained in [9] for a potential with a degenerate spinodal region, the new feature here is that island nucleation no longer occurs instantaneously but requires some time to develop. For example, the right island at $n = 3$ in Figure 15 starts forming already around $t = 29$, where one can see a bond inside the spinodal region, but it does not fully develop and start growing until a much later time, as can be seen from $t = 42$ snapshot, where the island has only grown by a few bonds (see also Figure 14(a)). The cascade island nucleation observed here is in agreement with the dynamic twin nucleation and growth due to lattice waves emitted by a sufficiently fast motion of a screw dislocation that was predicted in [28] and studied numerically in [29] and [30].

7. Concluding remarks

In this work, we used a simple antiplane shear lattice model with piecewise linear interactions to study the motion of a step propagating along a twin boundary. Following the approach developed in [15], we constructed semi-analytical traveling wave solutions for a wide range of the velocities and showed that the width of the spinodal region and the material anisotropy have a significant effect on the resulting kinetic relation between the applied stress and the velocity of the step. Our results extend and complement the work in [15, 25, 26] by considering slow step propagation that was not investigated previously. Our semi-analytical results and numerical simulations strongly suggest that such motion does not only exist but may become stable if the spinodal region is sufficiently wide. The slow step motion requires very small applied stress and involves emitted lattice wave that may propagate both behind and ahead of the moving step. This is in contrast to the previously studied high-velocity motion that features waves only behind the step and requires a larger stress. We also numerically investigated the solution breakdown when the applied stress is above a certain critical value. In this case the lattice waves emitted by the moving step and propagating behind it enter the spinodal region and lead to a cascade nucleation, growth and coalescence of multiple islands on top of the moving step. Compared to the similar results in [9], where the spinodal region was degenerate, in our case the island nucleation does not happen instantaneously.

The solution procedure was also used to find new admissible traveling wave solutions at low velocities in the case when the spinodal region degenerates to a single point. Applying the method in [27], we showed that these new solutions, in which the transforming bonds stay at the spinodal value before switching to the new twin variant, bifurcate from the solutions where the transition is instantaneous precisely at the threshold velocity where the latter become inadmissible. This allowed us to extend the kinetic relation in [13, 16] to lower velocities, where no admissible solutions were previously found.

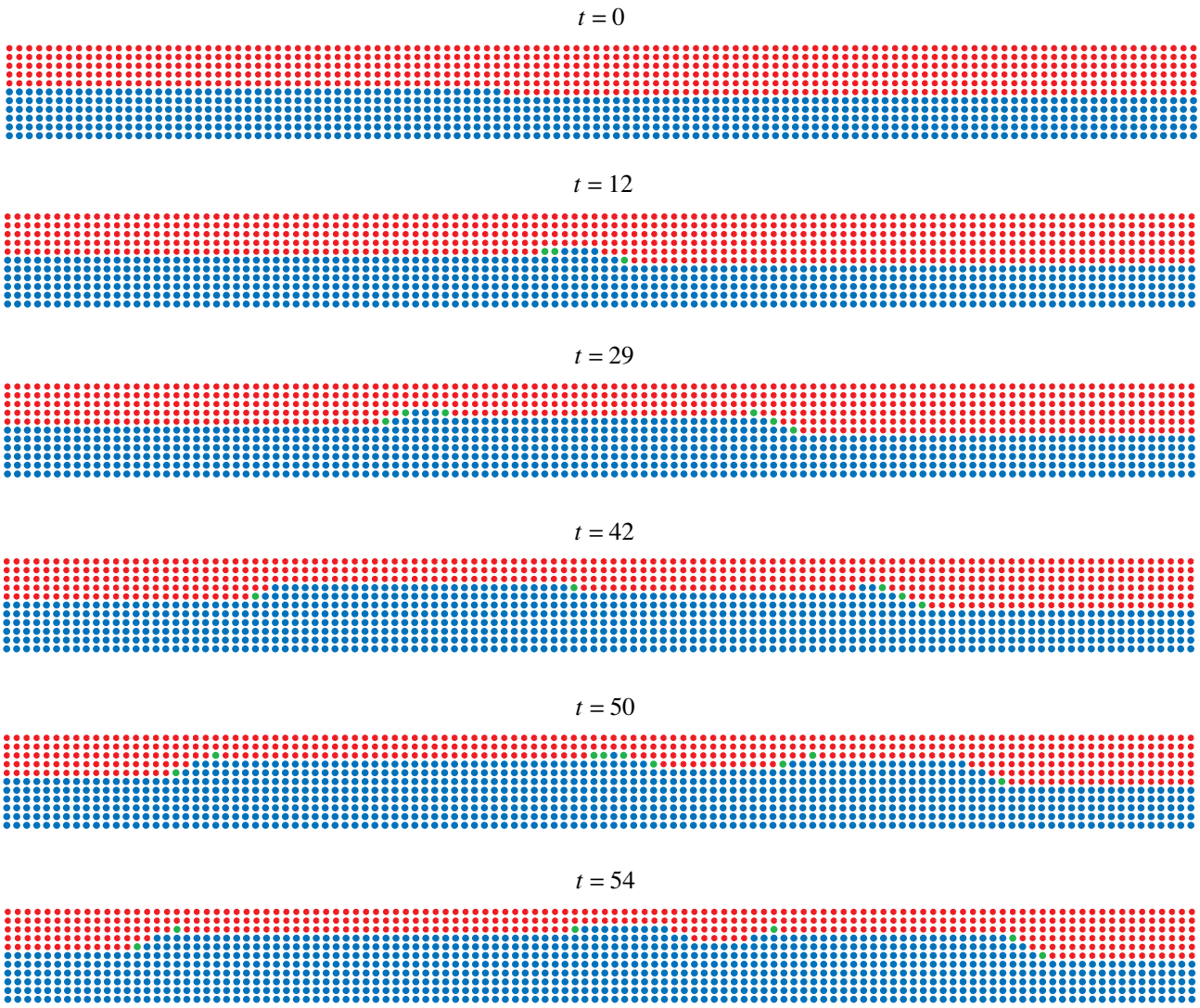

Figure 15. Time snapshots of island nucleation and growth at $\sigma = 0.45$, $\delta = 0.8$ and $\chi = 1$. The corresponding evolution of step fronts is shown in Figure 14(a). Here the blue points represent vertical bonds that have strain in variant II, the red ones are in variant I, and the green ones are in the spinodal region.

We remark that the kinetic relations obtained here are in general quantitatively different from the ones obtained in [23, 27] for the closely related one-dimensional FK model due to the different kernel (23) in the integral equation (25). In particular, the amplitude of the oscillations in our kernel decays at infinity [8], while in the one-dimensional case it remains constant. Note also that the one-dimensional problem has stronger singularities at the resonance velocities in the $z = 0$ case [16]. Nevertheless, qualitatively many of the results are similar, suggesting that the one-dimensional model, which is technically much less involved, captures the basic features of the kinetics of a single step. One important exception is the solution breakdown at high velocities in the present model, which is an essentially higher-dimensional phenomenon, since it involves step nucleation at $n \geq 2$.

This work can be extended to the case of multiple steps as in [8, 9] and to other lattice geometries. The ultimate challenge is the multiscale problem of obtaining the kinetic relation for a twin boundary from the step kinetics that takes into account the interaction between the steps.

Acknowledgement

We thank Yubao Zhen for many useful discussions and all the technical support he provided along with his computer code that was modified for this project.

Funding

This work was supported by the NSF (grant number DMS-1007908).

References

[1] Bhattacharya, K. *Microstructure of martensite*. Oxford: Oxford University Press, 2003.
[2] Bray, D, and Howe, J. High-resolution transmission electron microscopy investigation of the face-centered cubic/hexagonal close-packed martensite transformation in Co-31.8 WtPctNi alloy: part I. Plate interfaces and growth ledges. *Metll Mater Trans A* 1996; 27A: 3362–3370.
[3] Hirth, JP, and Lothe, J. *Theory of dislocations*. New York: Wiley, 1982.
[4] Hirth, JP. Ledges and dislocations in phase transformations. *Metll Mater Trans A* 1994; 25A: 1885–1894.
[5] Müllner, P, Chernenko, VA, and Kostorz, G. Stress-induced twin rearrangement resulting in change of magnetization in a Ni–Mn–Ga ferromagnetic martensite. *Scripta Mater* 2003; 49: 129–133.
[6] Abeyaratne, R, and Vedantam, S. A lattice-based model of the kinetics of twin boundary motion. *J Mech Phys Solids* 2003; 51: 1675–1700.
[7] Tsai, H, and Rosakis, P. Quasi-steady growth of twins under stress. *J Mech Phys Solids* 2001; 49: 289–312.
[8] Zhen, Y, and Vainchtein, A. Dynamics of steps along a martensitic phase boundary I: Semi-analytical solution. *J Mech Phys Solids* 2008; 56: 496–520.
[9] Zhen, Y, and Vainchtein, A. Dynamics of steps along a martensitic phase boundary II: Numerical simulations. *J Mech Phys Solids* 2008; 56: 521–541.
[10] Sharma, BL, and Vainchtein, A. Quasistatic propagation of steps along a phase boundary. *Cont Mech Thermodyn* 2007; 19(6): 347–377.
[11] Atkinson, W, and Cabrera, N. Motion of a Frenkel–Kontorova dislocation in a one-dimensional crystal. *Phys Rev A* 1965; 138(3): 763–766.
[12] Carpio, A, and Bonilla, LL. Oscillatory wave fronts in chains of coupled nonlinear oscillators. *Phys Rev E* 2003; 67: 056621.
[13] Celli, V, and Flytzanis, N. Motion of a screw dislocation in a crystal. *J Appl Phys* 1970; 41(11): 4443–4447.
[14] Earmme, YY, and Weiner, JH. Dislocation dynamics in the the modified Frenkel–Kontorova model. *J Appl Phys* 1977; 48(8): 3317–3341.
[15] Flytzanis, N, Crowley, S, and Celli, V. High velocity dislocation motion and interatomic force law. *J Mech Phys Solids* 1977; 38: 539–552.
[16] Ishioka, S. Uniform motion of a screw dislocation in a lattice. *J Phys Soc Japan* 1971; 30(2): 323–327.
[17] Kresse, O, and Truskinovsky, L. Mobility of lattice defects: discrete and continuum approaches. *J Mech Phys Solids* 2003; 51: 1305–1332.
[18] Marder, M, and Gross, S. Origin of crack tip instabilities. *J Mech Phys Solids* 1995; 43: 1–48.
[19] Slepyan, LI. *Models and Phenomena in Fracture Mechanics*. New York: Springer-Verlag, 2002.
[20] Slepyan, LI, and Ayzenberg-Stepanenko, MV. Localized transition waves in bistable-bond lattices. *J Mech Phys Solids* 2004; 52: 1447–1479.
[21] Slepyan, LI, Cherkaev, A, and Cherkaev, E. Transition waves in bistable structures. II. Analytical solution: wave speed and energy dissipation. *J Mech Phys Solids* 2005; 53: 407–436.
[22] Truskinovsky, L, and Vainchtein, A. Kinetics of martensitic phase transitions: Lattice model. *SIAM J Appl Math* 2005; 66: 533–553.
[23] Vainchtein, A. Effect of nonlinearity on the steady motion of a twinning dislocation. *Physica D* 2010; 239: 1170–1179.
[24] Vainchtein, A. The role of spinodal region in the kinetics of lattice phase transitions. *J Mech Phys Solids* 2010; 58(2): 227–240.
[25] Crowley, S, Flytzanis, N, and Celli, V. Dynamic Peierls stress in a crystal model with slip anisotropy. *J Phys Chem Solids* 1978; 39(10): 1083–1087.
[26] Flytzanis, N, Crowley, S, and Celli, V. Solitonlike motion of a dislocation in a lattice. *Phys Rev Lett* 1977; 39(14): 891–894.
[27] Rosakis, P, and Vainchtein, A. New solution for slow moving kinks in a forced Frenkel-Kontorova chain. *J Nonlin Sci* 2013; in press, submitted.
[28] Ishioka, S. Stress field around a high speed screw dislocation. *J Phys Chem Solids* 1975; 36: 427–430.
[29] Ishioka, S. Dynamic formation of a twin in a bcc crystal. *J Appl Phys* 1975; 46: 4271–4274.
[30] Koizumi, H, Kirchner, HOK, and Suzuki, T. Lattice wave emission from a moving dislocation. *Phys Rev B*. 2002;65:214104.
[31] Healey, TJ, and Miller, U. Two-phase equilibria in the anti-plane shear fo an elastic solid with interfacial effect via global bifurcation. *Proc R Soc A* 2007; 463: 1117–1134.
[32] Swart, PJ, and Holmes, PJ. Energy minimization and the formation of microstructure in dynamic anti-plane shear. *Arch Ration Mech Anal* 1992; 121: 37–85.
[33] Celli, V, Flytzanis, N, and Crowley, S. Analysis of the displacement field of a moving dislocation in a crystal. *J Phys Chem Solids* 1976; 37: 1125–1133.
[34] Ishioka, S. A theory of the Peierls stress of a screw dislocation. I. *J Phys Soc Japan* 1974; 36(1): 187–195.
[35] Cserti, J. Application of the lattice Green's function for calculating the resistance of infinite networks of resistors. *Am J Phys* 2000; 85(15): 896–960.

[36] Kratovchil, J, and Indenbom, VL. The mobility of a dislocation in the Frenkel–Kontorova model. *Czech J Phys B* 1963; 13: 891–894.
[37] Weiner, JH, and Sanders, WT. Peierls stress and creep in a linear chain. *Phys Rev* 1964; 134(4A): 1007–1015.

Appendix A: analytical expression for $\mathcal{J}$

Recall that the integral form of $\mathcal{J}(k_\xi, n)$ is given by (17). Note that $\mathcal{J}(k_\xi, n)$ has the symmetry property that for any integer n

$$\mathcal{J}(k_\xi, -n) + \mathcal{J}(k_\xi, n+1) = 0, \tag{39}$$

and hence only the case $n \geq 1$ needs to be considered. Following [13], we rewrite (17) as an integral over the unit circle in the complex plane:

$$\mathcal{J}(k_\xi, n) = \oint_{|\zeta|=1} \frac{(1-\zeta)\zeta^{-n}}{i(\zeta^2 - 2\lambda\zeta + 1)}\, d\zeta, \tag{40}$$

where $\zeta = e^{ik}$ and $\lambda(k_\xi)$ is given by (21). Applying the residue theorem to the integration in (40), we obtain an analytic expression:

$$\mathcal{J}(k_\xi, n) = \begin{cases} \pi(1 + \sqrt{\frac{\lambda-1}{\lambda+1}})(\lambda - \sqrt{\lambda^2-1})^{-n}, & \lambda < -1, \\ \pi(1 \mp i\sqrt{\frac{1-\lambda}{1+\lambda}})(\lambda \mp i\sqrt{1-\lambda^2})^{-n}, & |\lambda| < 1, \quad k_\xi \lessgtr 0, \\ \pi(1 + \sqrt{\frac{\lambda-1}{\lambda+1}})(\lambda + \sqrt{\lambda^2-1})^{-n}, & \lambda > 1. \end{cases} \tag{41}$$

We remark that the derivation of (41) for $|\lambda| < 1$ involves the poles $\zeta = \lambda \pm i\sqrt{1-\lambda^2}$ located on the unit circle $|\zeta| = 1$ (the path of integration in (40)), which correspond to the lattice waves emitted by the moving step. To resolve these singularities in a way that selects physically relevant solutions, we follow the approach in [13] and introduce a small damping contribution, which corresponds to replacing λ in (21) by $\lambda = \lambda_0 + i\gamma V k_\xi/2$, where λ_0 is given by the right-hand side of (21), $\gamma > 0$ is a small damping coefficient, and we recall that $V > 0$. Then for $|\lambda_0| < 1$ one of the poles shifts slightly outside the unit circle, while the other one shifts slightly inside the circle, depending on the sign of k_ξ. In the limit when $\gamma \to 0$ and thus $\lambda \to \lambda_0$, this means that the unit circle should be indented inward around $\zeta = \lambda - i\sqrt{1-\lambda^2}$ and outward around $\zeta = \lambda + i\sqrt{1-\lambda^2}$ when $k_\xi < 0$. Meanwhile, for $k_\xi > 0$ the opposite is true: the path of integration is indented inward around $\zeta = \lambda + i\sqrt{1-\lambda^2}$ and outward around $\zeta = \lambda - i\sqrt{1-\lambda^2}$. This ensures the selection of the relevant pole in the residue theorem calculation and results in a physically meaningful distribution of lattice waves in the final solution, in the sense that it is not destroyed in the presence of small damping. We observe that in [8], the expression corresponding to (41) has $\lambda'(k_\xi) \gtrless 0$ instead of $k_\xi \lessgtr 0$, which is equivalent in the region $V > V_1$ above the first resonance velocity that is studied in [8]. However, a formal extension of the formula in [8] to $V < V_1$ does not satisfy the above zero-damping limit criterion.

Using

$$\mathcal{S}(k_\xi, n) = \frac{\mathcal{J}(k_\xi, n+1) - \mathcal{J}(k_\xi, n)}{2\pi}, \tag{42}$$

(39) and (41), we then obtain the analytic expression (20) for $\mathcal{S}(k_\xi, j)$.

Appendix B: Equilibrium states and the Peierls stress

In this appendix, we consider the equilibrium states ($V = 0$), which are governed by the system of difference equations

$$\chi(u_{m+1,n} - 2u_{m,n} + u_{m-1,n}) + \Phi'(u_{m,n+1} - u_{m,n}) - \Phi'(u_{m,n} - u_{m,n-1}) = 0 \tag{43}$$

and correspond to the configuration such as that shown in Figure 2, i.e. satisfy

$$y_{m,n} < -\delta/2, \quad n \geq 2, \qquad y_{m,n} > \delta/2, \quad n \leq 0,$$

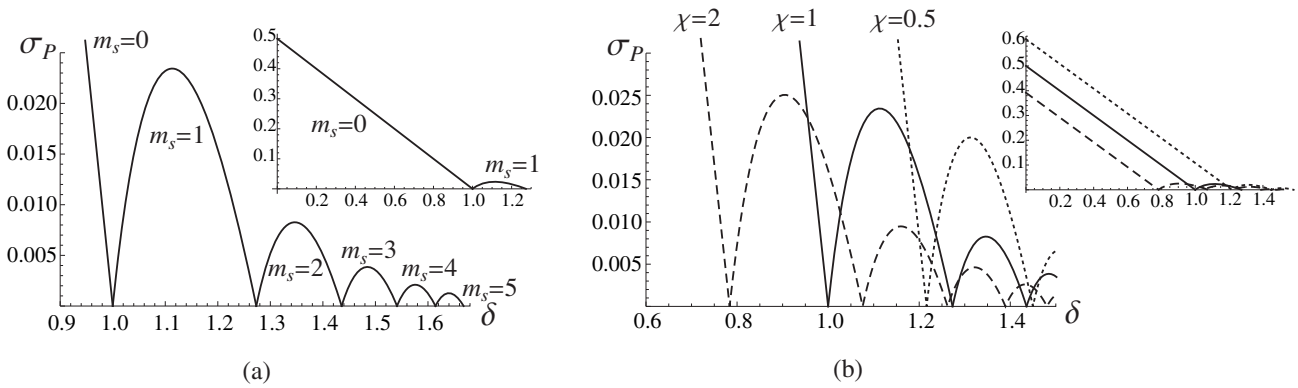

Figure 16. (a) Dependence of the Peierls σ_P stress on the width δ of the spinodal region at $\chi = 1$. Here m_s is the number of spinodal $n = 1$ vertical bonds in a stable equilibrium configuration, while an unstable equilibrium has $m_s + 1$ such bonds. (b) Plots of $\sigma_P(\delta)$ at $\chi = 2$ (dashed curve), $\chi = 1$ (solid curve) and $\chi = 0.5$ (dotted curve). Insets show the Peierls stress at smaller δ.

$$y_{m,1} \geq \delta/2, \quad m \leq 0, \qquad y_{m,1} \leq -\delta/2, \quad m \geq m_s + 1, \tag{44}$$

and

$$|y_{m,1}| \leq \delta/2, \quad m = 1, \ldots, m_s, \quad \text{if } m_s \geq 1,$$

where m_s is the number of $n = 1$ vertical bonds in the spinodal region. Under these assumptions, (43) become

$$\begin{aligned} &\chi(u_{m+1,n} + u_{m-1,n} - 2u_{m,n}) + u_{m,n+1} + u_{m,n-1} - 2u_{m,n} \\ &= -2\delta_{n,0} + (\delta_{n,0} - \delta_{n,1}) \left\{ 2\theta(-m) + \left(1 + \frac{2}{\delta}(u_{m,1} - u_{m,0})\right) [\theta(m_s - m) - \theta(-m)] \right\}, \end{aligned} \tag{45}$$

where the unit function satisfies $\theta(0) = 1$.

If $m_s = 0$, the displacement field can be obtained using the lattice Green's function as in [9, 35], yielding

$$u_{m,n} = \frac{1}{\pi\chi} \int_0^\pi \mathfrak{J}(m) \frac{\cos(n-1)\kappa - \cos n\kappa}{\sinh s}\, d\kappa, + \begin{cases} n(\sigma - 1), & n \geq 0, \\ n(\sigma + 1), & n \leq -1, \end{cases} \tag{46}$$

where $s \geq 0$ satisfies $\cosh s = (\chi + 1 - \cos\kappa)/\chi$ and

$$\mathfrak{J}(m) = \begin{cases} \frac{e^s + 1 - e^{ms}}{e^s - 1}, & m < 0, \\ \frac{e^{(1-m)s}}{e^s - 1}, & m \geq 0. \end{cases} \tag{47}$$

One can show that the solution (46) exists if and only if the applied stress is within the *trapping region* $|\sigma| \leq \sigma_P$, where

$$\sigma_P = 1 - \frac{\delta}{2} - \frac{2}{\pi} \int_0^\pi \mathfrak{J}(1) \frac{\cosh s - 1}{\sinh s}\, d\kappa.$$

is the Peierls stress at which $y_{1,1} \equiv u_{1,1} - u_{1,0} = -\delta/2$. For example, at $\chi = 1$ we obtain $\sigma_P = (1 - \delta)/2$.

Since the Peierls stress must be non-negative, the equilibrium solutions with no spinodal bonds exist only for sufficiently narrow spinodal regions, e.g. $0 \leq \delta \leq 1$ for $\chi = 1$. In particular, at $\delta = 0$, equation (46) yields the single stable equilibrium state with the assumed configuration for σ inside the trapping region. For $0 < \delta < 2$ there are solutions with at least one spinodal bond. In general, this problem can be reduced to that analyzed in [34] for a screw dislocation. Here we simply summarize the results. Let $\alpha(N)$ be the largest eigenvalue of the $N \times N$ matrix $\mathbf{A}$ with the entries $a_{i,j} = \mathcal{A}(i - j)$, where

$$\mathcal{A}(p) = \frac{1}{\pi} \int_0^\pi e^{-|p|s} \frac{\cosh s - 1}{\sinh s}\, d\kappa$$

and we set $\alpha(0) = 0$. Then for $0 < \delta < 2$ and $|\sigma| < \sigma_P$, there are two equilibrium states, a stable state with m_s spinodal bonds and an unstable state with $m_s + 1$ spinodal bonds, where m_s is uniquely determined from the inequality

$$\alpha(m_s) < \frac{\delta}{2} < \alpha(m_s + 1). \tag{48}$$

The two equilibria merge into a saddle point at $\sigma = \sigma_P$. For $m_s \geq 1$ the displacement field is then given by

$$\begin{aligned} u_{m,n} = &\sum_{j=1}^{m_s} \left(1 + \frac{2}{\delta} Y_j\right) \frac{1}{\pi\chi} \int_0^\pi e^{-|m-j|s} \frac{\cos(n-1)\kappa - \cos n\kappa}{2\sinh s}\, d\kappa \\ &+ \frac{1}{\pi\chi} \int_0^\pi \mathfrak{J}(m) \frac{\cos(n-1)\kappa - \cos n\kappa}{\sinh s} d\kappa + \begin{cases} n(\sigma - 1), & n \geq 0, \\ n(\sigma + 1), & n \leq -1. \end{cases} \end{aligned} \tag{49}$$

where $Y_j \equiv y_{j,1}, j = 1, \ldots, m_s$ are the strains in the spinodal bonds found by solving the linear system

$$Y_i = \frac{2}{\delta} \sum_{j=1}^{m_s} \mathcal{A}(i-j) Y_j + \frac{2}{\pi} \int_0^\pi \left[\mathfrak{J}(i) + \frac{1}{2} \sum_{j=1}^{m_s} e^{-|i-j|s} \right] \frac{\cosh s - 1}{\sinh s} d\kappa + \sigma - 1, \quad i = 1, \ldots, m_s. \tag{50}$$

To determine the Peierls stress, which corresponds to $y_{m_s+1,1} = -\delta/2$ in a stable equilibrium, define

$$N_S = \begin{cases} N/2 & \text{if} \quad \text{mod}\,(N,2) = 0 \\ (N+1)/2 & \text{if} \quad \text{mod}\,(N,2) = 1, \end{cases}$$

$N_A = N - N_S$,

$$\beta(N,j) = \begin{cases} 1/2 & \text{if} \quad \text{mod}\,(N,2) = 0 \text{ and } j = N_S \\ 1 & \text{otherwise,} \end{cases}$$

and let $\mathbf{B}_S(N)$ be the $N_S \times N_S$ matrix with the entries

$$(b_S)_{i,j} = \frac{\delta}{2}\delta_{i,j} - [\mathcal{A}(i-j) + \mathcal{A}(N+1-i-j)]\beta(N,j),$$

while $\mathbf{B}_A(N)$ is the $N_A \times N_A$ matrix with the entries

$$(b_A)_{i,j} = \frac{\delta}{2}\delta_{i,j} - [\mathcal{A}(i-j) - \mathcal{A}(N+1-i-j)].$$

We then obtain [34]

$$\sigma_P = -\frac{\det \mathbf{B}_S(m_s)}{\det \mathbf{B}_A(m_s)} \cdot \frac{\det \mathbf{B}_S(m_s+1)}{\det \mathbf{B}_A(m_s+1)}, \tag{51}$$

where for $m_s = 1$ and $m_s = 0$ the zero-size determinants equal 1. Figure 16 shows the dependence of Peierls stress on the width δ of the spinodal region at different χ. Note that the dependence on δ is no longer linear when spinodal bonds exist ($m_s \geq 1$). At $\delta = 2\alpha(m_s)$, $m_s = 1, 2, \ldots$, there is no trapping region, i.e. $\sigma_P = 0$. This is an artifact of the trilinear model and is not generic. Similar results were obtained for the FK model in [36, 37].